BIOCHEMISTRY
including biophysical chemistry & molecular biology

Article

pubs.acs.org/biochemistry

Conformational Characterization of Synapse-Associated Protein 97 by Nuclear Magnetic Resonance and Small-Angle X-ray Scattering Shows Compact and Elongated Forms

Mark D. Tully,[†] J. Günter Grossmann,[†] Marie Phelan,[†] Sravan Pandelaneni,[†] Mark Leyland,[‡] and Lu-Yun Lian*[,†]

[†]Institute of Integrative Biology, University of Liverpool, Liverpool L69 7ZB, U.K.

[‡]Department of Biochemistry, University of Leicester, Leicester LE1 9HN, U.K.

Supporting Information

ABSTRACT: Synapse-associated protein 97 (SAP97) is a membrane-associated guanylate kinase protein that interacts with other proteins such as ion channels, subunits of glutamate receptors, and other cytoskeletal proteins and molecular scaffolds. The molecular diversity of SAP97 results from alternative splicing at the N-terminus, and in the U1 and U5 regions. There are two main N-terminal isoforms: the β-isoform has an L27 domain, whereas in the α-isoform, this is replaced by a palmitoylation motif. We have used multiangle light scattering, nuclear magnetic resonance, and small-angle X-ray scattering studies to characterize the conformation of a truncated form of the β-isoform, hence mimicking the α-isoform. This paper provides a comprehensive view of the small-angle X-ray scattering data, and the resulting data show that the scattering data are consistent with the presence of an ensemble of forms in dynamic equilibrium, with two prominent populations of compact and extended forms, with R_g values of 38 ± 7 Å (52%) and 70 ± 10 Å (37%), respectively. The data show that without the L27 domain, the conformation of SAP97 is biased toward the compact form. We propose a hypothesis in which the overall conformation of SAP97 is determined by the nature of the N-terminus, which may, in turn, influence the specific role of a particular splice variant.

Synapse-associated protein 97 (SAP97), the mammalian homologue of the *Drosophila* discs-large tumor suppressor, is a member of the membrane-associated guanylate kinase (MAGUK) superfamily of proteins that interacts with a range of other proteins such as ion channels,[1] subunits of glutamate receptors,[2,3] cytoskeletal proteins,[4] kinases,[5] and other molecular scaffolds.[6] Like other MAGUK proteins, SAP97 is a multidomain protein, containing three PDZ domains and the SH3-GK domains. Linking the core conserved protein−protein interaction domains are five unique regions, U1−U5. The molecular diversity of SAP97 results from alternative splicing at the N-terminus, and in the U1 (I1A and I1B insertions) and U5 (between the SH3 and guanylate kinase domains with I3, I2, I5, and I4 insertions) regions.[7] The extensive alternative splicing in the U5 region produces isoforms that also affect AMPAR function, with the presence of the I3 insert increasing the level of AMPAR surface expression and activity.[5,8] This effect may be mediated by the ability of this splice variant to bind band 4.1 actin binding protein and CaMKII.[9] The I1A splice variant within the U1 region has also been shown to affect the activity and surface expression of voltage-gated K^+ channel Kv1.5.[10]

Two main isoforms have been reported in the N-terminal region: the predominant β-isoform that has the L27 oligomerization domain and the α-isoform, in which the first 100 amino acids of the β-isoform, including the L27 domain, are replaced by a palmitoylation motif.[11] This difference in the N-terminus appears to influence the subsynaptic distribution and function of SAP97; the α-isoform is targeted to the postsynaptic density, whereas the β-isoform is located in the nonpostsynaptic density, perisynaptic region where the L27 domain mediates heteromultimerization with other L27-containing proteins.[9] Consequently, the localization and dynamics of receptors such as the AMPA receptors that bind to SAP97 are influenced by the differential distribution of the SAP97 isoforms. As the AMPA receptors are the principal glutamatergic receptors in the mammalian excitatory synapse, the dynamics of their synaptic localization has a direct influence on synaptic strength. Therefore, mechanisms that determine AMPAR localization in the postsynaptic region will also influence how information is processed and stored in the brain.

Low-resolution EM and single-particle analyses of full-length SAP97 showed that the protein exists as a mixture of conformations, with ∼65% appearing as extended rodlike monomeric particles and the remaining 35% as C-shaped or ringlike structures,[12] the latter being similar to the conformation adopted by PSD-95. It would appear that the

Received: July 29, 2011
Revised: December 24, 2011
Published: December 27, 2011

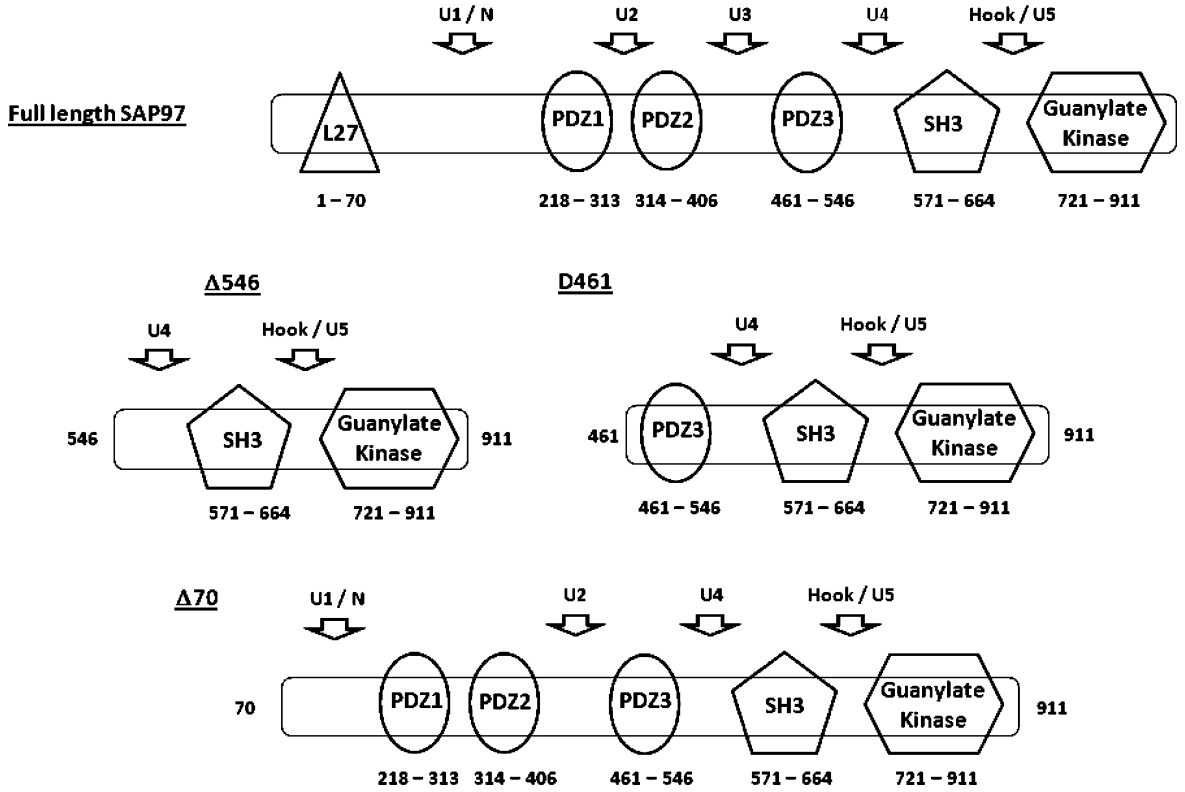

Figure 1. Schematic diagram of the domain organization of rat SAP97 highlighting the position of the relevant domains and of the recombinant SAP97 proteins (Δ70, Δ461, and Δ546) used in this study. The numbering system corresponds to the sequence of full-length rat SAP97.

conformations of MAGUKs are affected by the nature of the N-termini, with a preference for an elongated conformation when the L27 domain is present and a compact form in its absence. It may be that the conformation adopted by the MAGUK protein subtly determines the preferred binding partners.[12] Furthermore, because the MAGUK is a large, multidomain protein that is capable of interacting with a range of cellular proteins, it is likely that these interactions occur in a regulated manner.

Wu et al. proposed a model of the structure of full-length SAP97 and a description of how calmodulin binding might influence the overall structure and conformation of SAP97.[13] However, a revision of the modeled structure is needed in light of the experimentally determined high-resolution data that are now available for several regions of the protein. For example, the N-terminal region forms the highly helical L27 domain[14] rather than the proposed β-sheet fibronectin domain. The SH3-GK structure for the homologous PSD-95 shows that this is a "single" domain consisting of two regions, one adopting an SH3 fold and the other a guanylate kinase (GK) fold, with intimate intramolecular interactions between the two regions.[15,16] In addition, our NMR studies of the conformation of the triple PDZ of SAP97 show that the U3 region is predominantly unfolded, rather than the proposed β-sheet.[17]

Here, we report a detailed analysis, using multiangle light scattering (MALLS), NMR, and small-angle X-ray scattering (SAXS), of the conformations of truncated SAP97 in which the L27 domain has been removed from rat βSAP97, to mimic the α-isoform of SAP97 and full-length PSD-95. The truncated protein [hereafter simply Δ70 (Figure 1)] was essentially a monomer. This work elucidates the structure of truncated SAP97. The NMR analyses show that the N-terminal region between the L27 domain and the first PDZ domain (part of the U1 region) is unstructured. The NMR data for Δ70, Δ461 (consisting of PDZ3 and the SH3-GK region), and Δ546 (comprising only the SH3-GK region) reveal that the PDZ region is more mobile than the SH3-GK domain. This work also describes how detailed analyses of SAXS data using both conventional techniques and the ensemble-optimized method (EOM) reveal that Δ70 exists in solution as a mixed population of fully extended, semiextended, and compact conformations, whereas the SH3-GK region of Δ546 exists predominantly in compact form. We propose from the results obtained here that the isoform-dependent distribution of SAP97 in the synapse also reflects a separation of conformations, with the predominantly compact form located in the synapse and the extended form in the perisynapse.

EXPERIMENTAL PROCEDURES

Expression and Purification of SAP97 Domains. Truncated versions of rat βSAP97 containing the I1b, I3, and I5 splice inserts were amplified via polymerase chain reaction from plasmid pEGFP-SAP97 (a gift from C. C. Garner, Palo Alto, CA). The genes were inserted into vector pLEIC-01, a T7 Lac-operon vector including an N-terminal hexahistidine purification tag followed by a TEV cleavage site. The amino acid sequences of the various constructs are given in Figure S1 of the Supporting Information; in broad terms, Δ70 is full-length βSAP97 with the first 70 amino acids deleted, Δ461 encompasses the PDZ3 and SH3-U5-GK domains, and Δ546 consists of the SH3-U5-GK domains. SAPN consists of residues 70−311 encompassing part of the N-terminal region and the first PDZ domain; GK consists of residues 721−900. Unless otherwise stated, all proteins were expressed and purified using similar conditions. The plasmids expressing the different domains were transformed into BL21(DE3) cells (Novagen),

dx.doi.org/10.1021/bi201178v | *Biochemistry* 2012, 51, 899−908

grown in LB or ^{15}N-labeled minimal medium containing 0.1 g/L ampicillin, induced with 1 mM IPTG, and left to grow overnight at 18 °C. Cells were pelleted, resuspended, lysed with a French press, filtered, and purified using a 5 mL HisTrap High Performance (GE Healthcare) column, followed by a 5 mL HiTrap Q FF anion exchange column (GE Healthcare). The sample was eluted using a 0 to 500 mM KCl gradient at a flow rate of 2 mL/min. Following concentration, the SAP97 samples were loaded onto either a 26/60 Superdex 75 (for Δ546 and Δ461) or a Superdex 200 (for Δ70) size-exclusion column pre-equilibrated with 500 mM NaCl, 50 mM Tris-HCl, 2 mM DTT, and 1 mM EDTA (pH 7.5). Isocratic elution yielded the desired protein. The peak fractions were concentrated with an Amicon filter (10K molecular weight cutoff). The protein samples were deemed to be >95% pure using a sodium dodecyl sulfate−polyacrylamide gel electrophoresis gel. Protein samples were identified by mass spectrometry.

Uniformly ^{2}H-labeled SAP97 and ^{15}N-labeled SAP97 were in media containing [^{15}N]ammonium chloride in a 2×M9 minimal medium (MM) prepared in D_2O rather than H_2O. More details of the protein purification are given in the Supporting Information (S5).

Size Exclusion Chromatography−Multiangle Laser Light Scattering (SEC−MALLS). Proteins were run on either a Superose 6 or a Superose 12 HR 300 mm × 10 mm gel filtration column (GE Healthcare Life Sciences) equilibrated in 50 mM phosphate and 50 mM NaCl (pH 6.8) at a rate of 0.71 mL/min. Elution was monitored with a Wyatt EOS 18-angle laser photometer (Wyatt Technology, Santa Barbara, CA), an Optilab rEX refractive index detector, and a Jasco (Easton, MD) UV-2077 Plus UV/vis spectrophotometer; these were coupled to a quasi elastic light scattering (QELS) detector for simultaneous measurement of hydrodynamic radii. Molar mass measurements were performed using both Astra version 5.3.2.16 (Wyatt Technology) and the "three-detector method". Values of mass and hydrodynamic radius are expressed as means ± the standard error (SE).

NMR Experiments. NMR samples at concentrations 0.2−0.5 mM were created in 50 mM Tris, 50 mM NaCl, and 1 mM NaN_3 in a 90% H_2O/10% D_2O mixture (pH 6.8). Unless otherwise stated, spectra were recorded at 25 °C using Avance Bruker 600 and 800 MHz spectrometers fitted with a triple-resonance, single-z-axis gradient cryogenic probehead. ^{1}H, ^{13}C, and ^{15}N resonance assignments of the SAPN were determined using the standard suite of triple-resonance experiments: CBCA(CO)NH, CBCANH, HNCA, HNCO, HN(CA)CO, and HN(CO)CA. The spectra were processed using Topspin (Bruker) and analyzed using CCPN Analysis. Chemical shift indexing was performed.

SAXS Experiments. Synchrotron SAXS data were collected on the SWING beamline at the SOLEIL Synchrotron (Paris, France). Samples were measured at concentrations of 1−5 mg/mL in 150 mM NaCl with 5 mM DTT (to prevent radiation damage). The temperature was held at 16 °C. The momentum transfer range, q, was set to 0.07−0.5 Å^{-1}, where $q = 4\pi \sin\theta/\lambda$, where 2θ is the scattering angle and λ the X-ray wavelength of 1.03 Å. Samples were centrifuged to remove particulates, and approximately 100 μL was loaded onto a high-performance liquid chromatography (HPLC) (Agilent) vial. For Δ546, the batch mode was used for data collection; in this method, a 40 μL sample was injected directly into the capillary flow cell, flanked by two bubbles of air. For Δ70, the sample was first passed through an online HPLC system before entering the flow cell. For both, data were collected in 255 time frames with 3 s per frame (13 min in total). The scattering images were averaged using beamline-specific software (Foxtrot) and the buffer scattering intensities subtracted using PRIMUS.[18] GNOM[19] was used to evaluate the radius of gyration (R_g), maximum molecular dimension D_{max}, and distance distribution function $P(r)$. Ab initio reconstruction of the particle shapes at low resolution was conducted using GASBOR,[20] which represents the protein as a chain of dummy residues centered at the Cα positions. An averaged and filtered representative model from 10 independent GASBOR models was generated using DAMAVER,[20] with no rejections for both constructs Δ546 and Δ70. CRYSOL was used to simulate scattering profiles from atomic coordinates.[21] The web server I-TASSER[22] was employed to generate an atomic structure of Δ546 using as a template the structure of the PSD-95 SH3-GK domain [Protein Data Bank (PDB) entry 1KJW]. Rigid-body modeling of the folded domains against the scattering data was performed using BUNCH[23] and EOM[24] to explore the range of possible conformations caused by the presence of flexible, unstructured polypeptide regions linking the folded PDZ and SH3-GK domains. The BUNCH model of Δ546 with the best goodness-of-fit value was used in subsequent rigid-body calculations for Δ70, in which the position of the SH3-GK moiety was fixed. The approach of ensemble optimization (EOM) determines an ensemble of structures from an initial pool of 10000 random conformers. A genetic algorithm selects an assortment of structural models whose average scattering profile is in close agreement with the experimental data. For Δ546, the predicted Δ546 BUNCH model structure was used as input for EOM. In the case of Δ70, the starting model for EOM was constructed by combining the Δ546 BUNCH model for the SH3-GK domain with the known crystal structures of SAP97 PDZ12 (PDB entry 3GSL) and PDZ3 (PDB entry 2PDR). EOM calculations were repeated five times to assess the consistency of ensemble mixtures.

RESULTS

MALLS Characterization of Δ70, Δ461, and Δ546. Purified recombinant Δ70, Δ461, and Δ546 (all containing the hexahistidine tag together with 16 additional amino acids) were all subjected to multiangle laser light scattering (MALLS) analyses. The traces for each of these proteins are shown in Figure 2. In all cases, the protein has approximately the same molecular mass across the whole peak in the chromatogram, with the reported M_n, M_w, and M_z values being very similar and the polydispersity being 1.000. The estimated molecular masses for Δ70, Δ461, and Δ546 from the MALLS experiments are 95540 ± 2866, 53230 ± 1596, and 46670 ± 1400 Da, respectively, all in close agreement with the expected monomeric molecular mass (Table 1). An initial analysis of the hydrodynamic data (R_h) suggests that Δ70 appears to be more elongated than either Δ461 or Δ546. However, the R_h values of Δ461 and Δ546 indicate only that these two proteins are shorter than Δ70 because both Δ461 or Δ546 are outside the detection limits of the MALLS technique for the precise determination of the R_h values. The translation diffusion moment of Δ70 is ∼5.61 × 10^{-7} cm^2/s, a value that is higher than the average for a protein of this size, again suggesting that Δ70 does adopts a somewhat extended conformation.

NMR Spectroscopy of the N-Terminal Region of SAP97. The region between the L27 domain and the first

dx.doi.org/10.1021/bi201178v | Biochemistry 2012, 51, 899−908

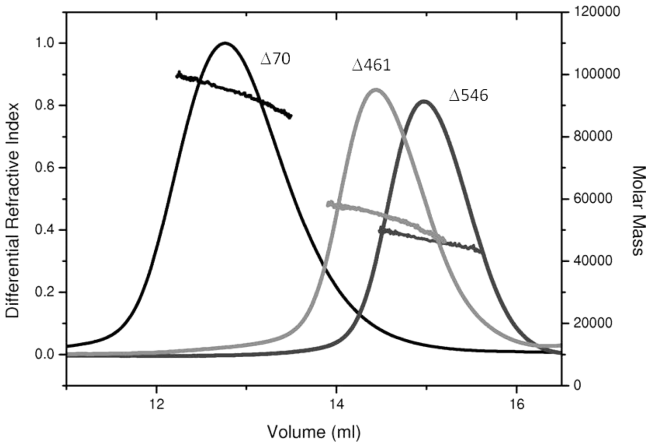

Figure 2. SEC−MALLS analysis of SAP97 domains. Shown is an expanded view of the differential refractive index chromatogram, including the molecular masses (M) of the proteins (black circles). The molecular masses of Δ70, Δ461, and Δ564 are 95540 ± 2866, 53230 ± 1596, and 46670 ± 1400 Da, respectively (experimental errors from polydispersity).

PDZ domain contains the I1B insertion (Figure S1 of the Supporting Information). To obtain stable and soluble protein, we expressed the region between residues 70 and 311 (SAPN), which includes the first PDZ domain (amino acids 218−311). The $^{15}N-^{1}H$ HQSC spectrum clearly showed resonances from PDZ1[17] in addition to very intense and poorly dispersed resonances. The backbone resonances from residue 70 to 218 were fully assigned. The chemical shift indices[25] suggest that this region does not adopt a stable, folded conformation (Figure S2 of the Supporting Information), although this region had previously been predicted to adopt a β-sheet conformation.[13]

NMR Characterization of Δ70, Δ461, and Δ546. The $^{15}N-^{1}H$ TROSY spectra of all three constructs are shown in Figure 3. The qualities of the Δ70 and Δ461 spectra are good for their sizes, and by overlaying these spectra with the spectra of the individual PDZ3 domain (for Δ461) or of the spectrum of residues 218−577, which includes the PDZ1, PDZ2, U3, PDZ3, and U4 domains (here termed PDZ123), we were able to discern which resonances are from the PDZ regions and which are from the SH3-GK region. The spectrum of Δ546 is of much poorer quality, with line widths much broader than those of the spectra of Δ70 and Δ461 even when the sample was deuterated. Nevertheless, it is possible, through a series of overlays, including the spectra of the PDZ domains, to identify many of the SH3-GK resonances from the spectra of Δ70 and Δ461. The spectrum of the isolated GK domain overlays poorly with the spectrum of either Δ546 or Δ461. It is only possible to obtain a partial assignment for the GK domain because the sample was unstable and precipitated at concentrations of >0.5 mM and at temperatures between 15 and 30 °C. For both Δ70 and Δ461, therefore, the resonances from the folded PDZ and unfolded regions (U1, U3, and U4) are identified by transferring the resonance assignments from the smaller domains;[17] the remaining, dispersed resonances are ascribed to residues from the SH3-GK domain without specific resonance assignments.

One interesting feature that is apparent in the spectra of Δ70 and Δ461 is the higher sensitivities of the resonances from the PDZ region compared with those from the SH3-GK domain, a difference that is much more obvious in the $^{15}N-^{1}H$ HSQC spectrum than in the TROSY spectrum. An analysis of these line widths in the TROSY spectra is shown in Figure 3D. The resonance volumes and/or intensities of randomly selected resonances from the PDZ region and the SH3-GK regions are clearly different despite the fact that the sizes of these two regions are similar. These results provide the first indication that the PDZ region is mobile with respect to the SH3-GK region. The poor sensitivity of the SH3-GK resonances is presumably due to unfavorable tumbling of this domain caused by its characteristic shape.

SAXS Studies of Δ70 and Δ546. SAXS experiments were performed on Δ70 and Δ546 in 150 mM NaCl. The Guinier analysis of the SAXS data reveals a linearity in the plots of the natural logarithm of the scattered intensity $I(q)$ versus q^2 for the condition $q < 1.3/R_g$ (see the insets of Figure 4A,B). This behavior indicates well-behaved samples and the absence of protein aggregation or polydispersity. In agreement with the MALLS data, the SAXS experiments therefore confirm the homogeneity and monodispersity of both samples in solution. The values of R_g and D_{max} obtained for the two constructs indicate that both Δ70 and Δ546 are rather nonspherical and elongated on average (Table 1). This becomes evident on the basis of a comparison with perfectly spherical molecules with these R_g values; such particles would possess D_{max} values of 111 Å (Δ70) and 75 Å (Δ546). The $P(r)$ curves depict the distribution of intramolecular atomic distances within the molecule and present distinct features. For Δ546, the asymmetrical $P(r)$ curve indicates a globular molecular core with a noteworthy tail possibly implying a small, elongated extension (Figure 4A). In the case of Δ70, the more distinctive, asymmetrical curve indicates a stretched out conformation (Figure 4B) with maxima at ∼80 and ∼110 Å suggesting at least two additional discrete globular domains. The D_{max} for

Table 1. Parameters Calculated from SAXS and MALLS Data[a]

	SAXS			SEC−MALLS	
	R_g (Å)	D_{max} (Å)		M_r (Da)	R_h (Å)
Δ70	42.9 ± 0.5	150 ± 7	Δ70	93720 ± 3%	43 ± 0.3
Δ70 (EOM)	37 (52.3%), 68 (23.0%), 78 (13.7%)				
			Δ461	53230 ± 3%	
Δ546	29.2 ± 0.3	115 ± 5	Δ546	46670 ± 3%	
Δ546 (EOM)	26.3 ± 2 (60.2%)				
	31.8 ± 2 (39.4%)				

[a]All methods and conditions are given in Experimental Procedures. The experimental data were determined by multiangle laser light scattering (MALLS) and small-angle X-ray scattering (SAXS). R_g is the radius of gyration, R_h the hydrodynamic radius, M_r the molecular mass, and D_{max} the maximum molecular dimension. Δ461 and Δ546 are too small for reliable determination for R_h values using the MALLS technique.

dx.doi.org/10.1021/bi201178v | Biochemistry 2012, 51, 899−908

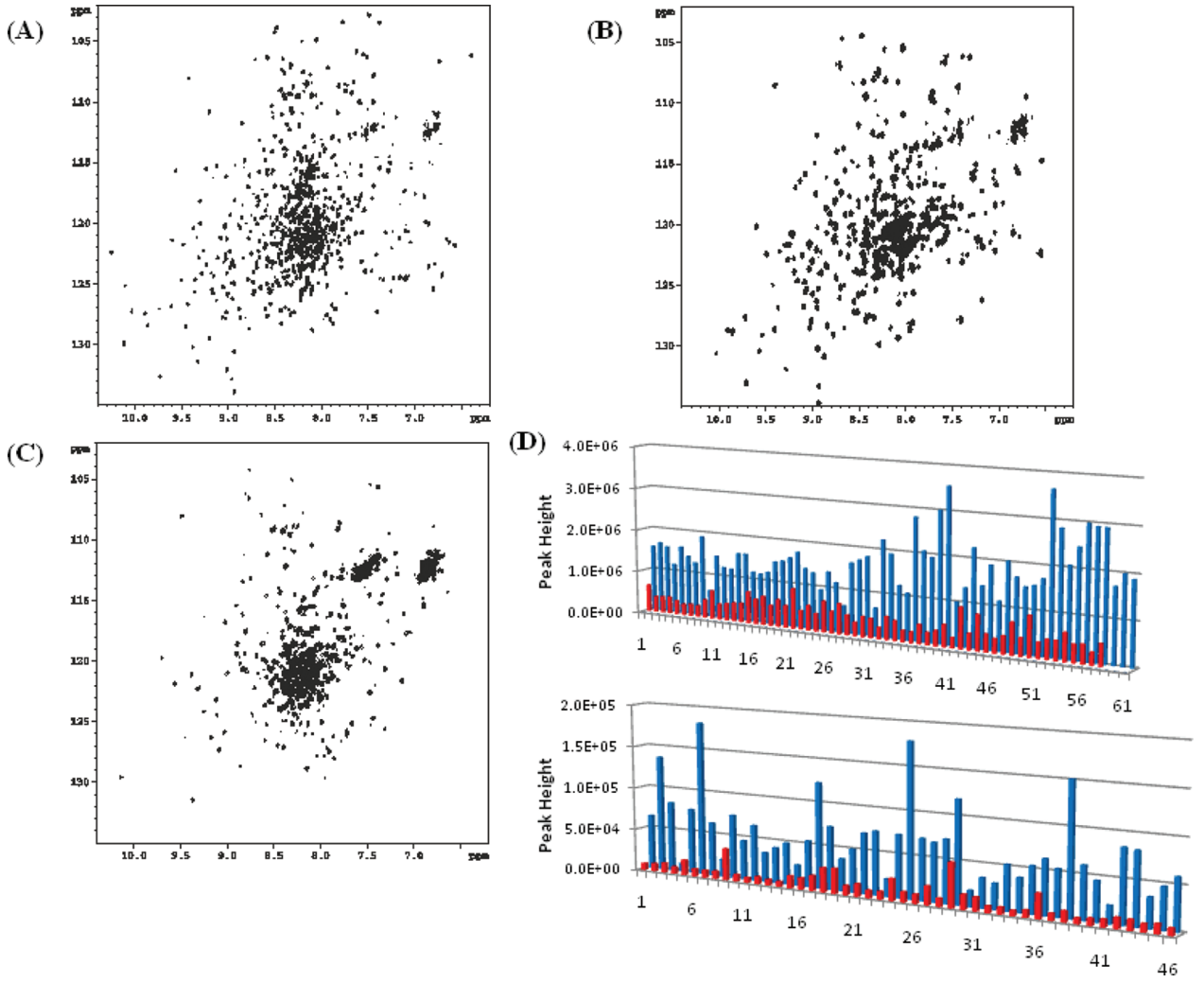

Figure 3. NMR spectra of SAP97. (A) $^{15}N-^{1}H$ TROSY spectrum of Δ70. (B) $^{15}N-^{1}H$ TROSY spectrum of Δ461. (C) $^{15}N-^{1}H$ TROSY spectrum of Δ564. (D) Comparison of the intensities of resonances of the SH3-GK domain (red) and the PDZ region (blue) for Δ70 (top) and Δ461 (bottom). For Δ70, the intensities for previously assigned resonances from PDZ1, -2, and -3 domains are used, and for Δ461, the intensities from the PDZ3 domain are used.[17]

Δ70 is ∼150 Å, which is consistent with a protein of this mass and agrees with the value derived from negative-stain electron microscopy for an extended, rodlike conformation of SAP97.[12] The R_g values obtained from the SAXS data are consistent with the R_h values determined via MALLS (Table 1).

Three-Dimensional (3D) Shape Analysis of Δ546. Several independent ab initio low-resolution shape models were restored with GASBOR.[20] All 10 low-resolution bead models (Figure S3 of the Supporting Information) showed a larger compact area with a smaller protrusion at one end. This protrusion can most likely be identified as the 63-amino acid N-terminal region consisting of the hexahistidine tag and the U4 linker region (see Figure S1 of the Supporting Information). The average 3D shape of Δ546 is presented in Figure 4C with the superimposed rigid-body model deduced with BUNCH.[23] Several rigid-body models obtained with BUNCH match each other well, with the exception of the N-terminal His-tagged U4 linker region, which can exist in a variety of arrangements. The Hook domain linker can be modeled to lie between the SH3 and GK domains. However, as individual rigid-body models (as reconstructed with BUNCH) do not provide excellent fits to the experimental scattering data, it is apparent that no unique structure is fully able to describe the experimental findings. We, therefore, analyzed the structural dynamics of Δ546 in light of mixtures of conformational states as implemented in the ensemble optimization method (EOM).[24] This method evaluates likely conformational variations and particularly applies to the study of monomeric multidomain proteins. No prior knowledge of the organization of these individual domains is needed. In the absence of a known crystal structure of SAP97, this method merely requires atomic models of individual domains. Therefore, the structure of Δ546 was modeled on the SH3-GK domain of PSD-95 (PDB entry 1JKW).[16] For subsequent calculations, this double domain was defined as one integral unit to maintain established interactions between the SH3 and GK domains.

From the initial 10000 random conformers generated for Δ546, EOM selected the ensemble of conformers presented in Figure 5, providing a very good fit to the experimental scattering data (goodness-of-fit value $\chi^2 = 4.8$) (Figure 5A). A frequency distribution of the conformers as a function of R_g is shown in Figure 5B. The EOM-optimized ensemble consists primarily of conformers in a compact population (∼60%) with an average R_g of ∼26.3 ± 2 Å. The remaining conformers show

dx.doi.org/10.1021/bi201178v | *Biochemistry* 2012, 51, 899−908

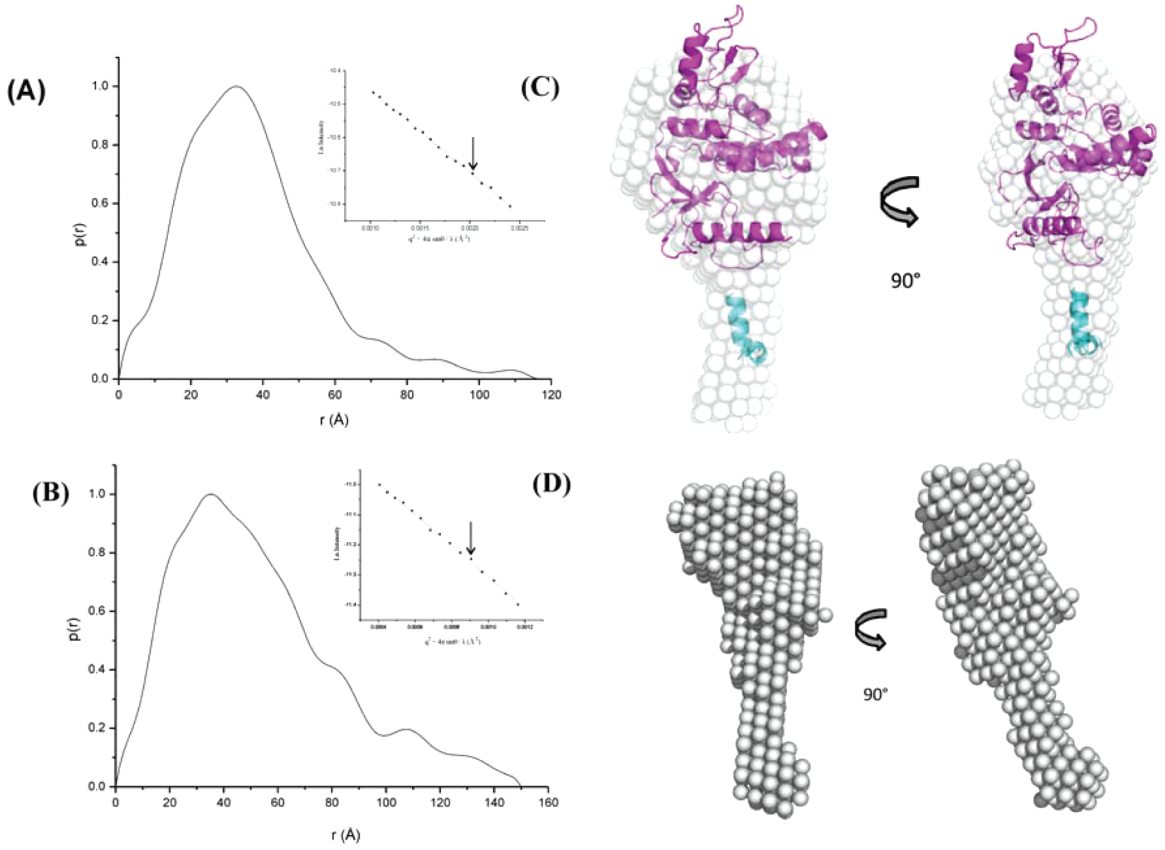

Figure 4. SAXS data for SAP97. $P(r)$ plots from the small-angle X-ray scattering of (A) Δ564 and (B) Δ70. For Δ546, the scattering data are averaged for samples at 1, 2, and 3 mg/mL. The $P(r)$ value (regularization parameter) is calculated by GNOM and gives an R_g of 29.2 Å and a D_{max} of 115 Å. For Δ70, the averaged scattering data are for 5 mg/mL protein passed through an HPLC system. The estimation of the $P(r)$ function was conducted with GNOM and gives an R_g of 42.9 Å and a D_{max} of 150 Å. The insets of panels A and B represent the corresponding Guinier plots emphasizing the homogeneity of the respective samples. The $q_{max} < 1.3/R_g$ condition used in the Guinier analysis is given by an arrow identifying q_{max}. (C) BUNCH model overlay with the average GASBOR shape model of Δ546 calculated with DAMAVER. (D) Average GASBOR shape model of Δ70 calculated with DAMAVER.

a protein elongated by an extended N-terminal region. Of particular note is the fact that the SH3-GK domain remains compact for all calculated conformers (Figure 5C). The N-terminus consists of the hexahistidine tag and the TEV cleavage site followed by the U4 linker region, which comprises an α-helix (residues 515−528) followed by a very short β-region (residues 529−532) (henceforth termed the $\alpha\beta$ region).[17] It is interesting to note that in ∼60% of the conformers, the $\alpha\beta$ region stays close to the SH3 domain (Figure 5B). The R_g value for the compact conformation concurs well with the experimental R_g value as well as the R_h value obtained from multiangle laser light scattering (MALLS) data, which also support a mostly compact structure.

The EOM analyses, therefore, show that the SH3-GK domain of SAP97 adopts a compact conformation with little mobility between the two domains; the 21-amino acid insertion (I3 and I5) does not appear to have an effect on the intimate interactions between the SH3 and GK domains, leaving the SAP97 SH3-GK domain to adopt essentially the same conformation found for the PSD-95 SH3-GK domain.

3D Shape Analysis of Δ70. Ten ab initio low-resolution 3D shape models were reconstructed from the experimental scattering profile (see Figure S4 of the Supporting Information) and show a larger main scattering mass with a drawn out area that is either collinear or at an angle to the core shape envelope. The average shape model is presented in Figure 4D and highlights a larger central mass with a long protrusion; we identified the core of the shape to belong to the PDZ3-SH3-GK domains and the protruding arm to specify the N-terminal segment encompassing the PDZ1 and PDZ2 domains and the U3 linker. Rigid-body modeling with BUNCH did not lead to satisfactory fits to the experimental scattering data. Hence, the ensemble optimization approach was used to assess the conformational heterogeneity of Δ70 in solution. An initial structure of Δ70 was based on an earlier rigid-body model of the SAP97 SH3-GK domain; atomic structures for the three PDZ domains consisted of PDB entry 3GSL for PDZ12 and PDB entry 2PDR for PDZ3. The fit of the ensemble scattering is in good agreement with the experimental data [$\chi^2 = 6.6$ (see Figure 6A)]. Representative models of the ensemble of conformers deduced by EOM fitting the experimental scattering data are presented in Figure 6B along with a frequency distribution as a function of R_g. Strikingly, two populations of conformers for Δ70, one with an R_g of 38 ± 7 Å (52%) and one with an R_g of 70 ± 10 Å (37%), dominate the resulting distribution. Despite the broad range of R_g values (and concomitant variation of 3D shapes), two predominant populations of conformers are clearly discernible, one of which is nearly twice as extended as the other. In the compact form, PDZ3 (cyan) is in the proximity of the SH3-GK domain, with the U4 region in a collapsed conformation (Figure 6B). In the elongated form, the SH3-GK, PDZ3, and PDZ1-PDZ2

dx.doi.org/10.1021/bi201178v | *Biochemistry* 2012, 51, 899−908

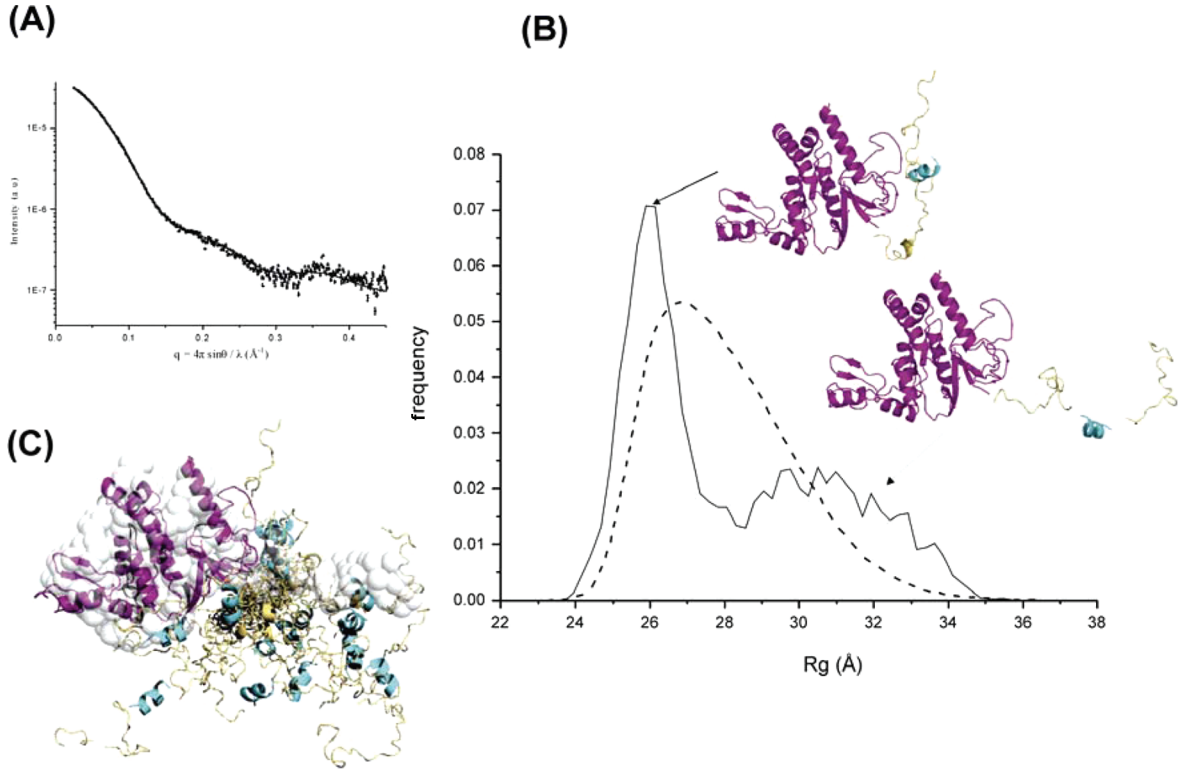

Figure 5. Analysis of SAXS data of Δ546 by the ensemble optimization method. (A) SAXS intensities plotted as a function of momentum transfer. Dots with error bars represent experimental data; the solid line corresponds to the fit obtained from the ensemble of 14 conformers. (B) Distribution of the selected conformers (solid line) and the initial pool of random structures (dashed line) as a function of R_g. Two representative structures for the conformers within the EOM ensemble were judged to realistically fit the Δ546 model. (C) EOM conformers superimposed on the SH3-GK domain and overlay on one GASBOR shape calculated ab initio to show the conformational variety for the N-terminus that contains the α-helix in the U4 region (cyan). The figure also shows that it is possible to fit one EOM model to the ab initio 3D shape model deduced with GASBOR. The ensembles of conformations produced from EOM fit the experimental scattering profile better than each individual model produced with BUNCH. Furthermore, EOM is able to model the flexible N-terminus more adequately. Color code: magenta for SH3-GK, cyan for the α-region, and yellow for the linker regions.

domains are separated by extended conformations of the U3 and U4 linkers. As highlighted above, we previously reported that the first half of U4 adopts an αβ structure; this could explain the preponderance of the collapse conformation of U4, which brings PDZ3 close to the SH3-GK domain in the calculated ensemble. In addition, we showed that the U3 region is dynamic but conformationally restricted and constraints the separation between the PDZ3 and PDZ12 domains. Interestingly, the low-resolution EOM structures suggest that even the compact structures are able to tether target proteins because the ligand binding sites do not appear to be occluded by neighboring domains. The EOM analyses, therefore, show that Δ70 folds into a mixture of compact and extended conformations with a very small population existing in the semiextended form.

DISCUSSION

Previous electron microscopy work suggested that SAP97 can adopt both bent and elongated conformations.[12] Molecular modeling also postulated a regulatory mechanism involving the binding of another protein such as calmodulin or protein 4.1.[13] The crystal structures of the SH3-GK domain of PSD-95[15,16] and other SH3-GK domains of the voltage-gated calcium channel[26,27] showed that the SH3-GK domain adopts a complicated split domain configuration, with the SH3 domain consisting of two subdomains, the second comprised of a distal β-sheet consisting of two-antiparallel β-strands. The two subdomains are separated by an intervening GK domain. Biochemical analyses using dissected domains from SAP97 revealed the possibility of SAP97 forming intramolecular interactions. Self-association through SH3-mediated interactions involving polyproline regions found in the N-terminal region of the polypeptide chain, in the I1A and I1B splice insertion, are also reported.[7] Furthermore, self-association was also postulated to occur via an "intermolecular" exchange of the second subdomains of the SH3 domain to reconstitute an intermolecular SH3 domain.[16] There are, however, little structural data to support these intra- and intermolecular interactions.

The NMR chemical shift indices show that the N-terminal region between the L27 and first PDZ domains is flexible and does not adopt a stable conformation. In terms of size, the PDZ domain-containing segment including the N-terminal domain and the U3 region accounts for more than 50% of the intact SAP97 molecule, yet the NMR line widths for this segment are much narrower than the residues from the SH3-GK domain. The data show that the folded PDZ region is mobile and tumbles in a manner that is independent of the SH3-GK domain and at a different time scale. This higher mobility of the PDZ domain-containing region is most likely due to the flexibility of linker regions U3 and U4, accompanied by the presence of only very weak contacts between the PDZ3 domain and the PDZ1-PDZ2 didomain.[17]

dx.doi.org/10.1021/bi201178v | Biochemistry 2012, 51, 899−908

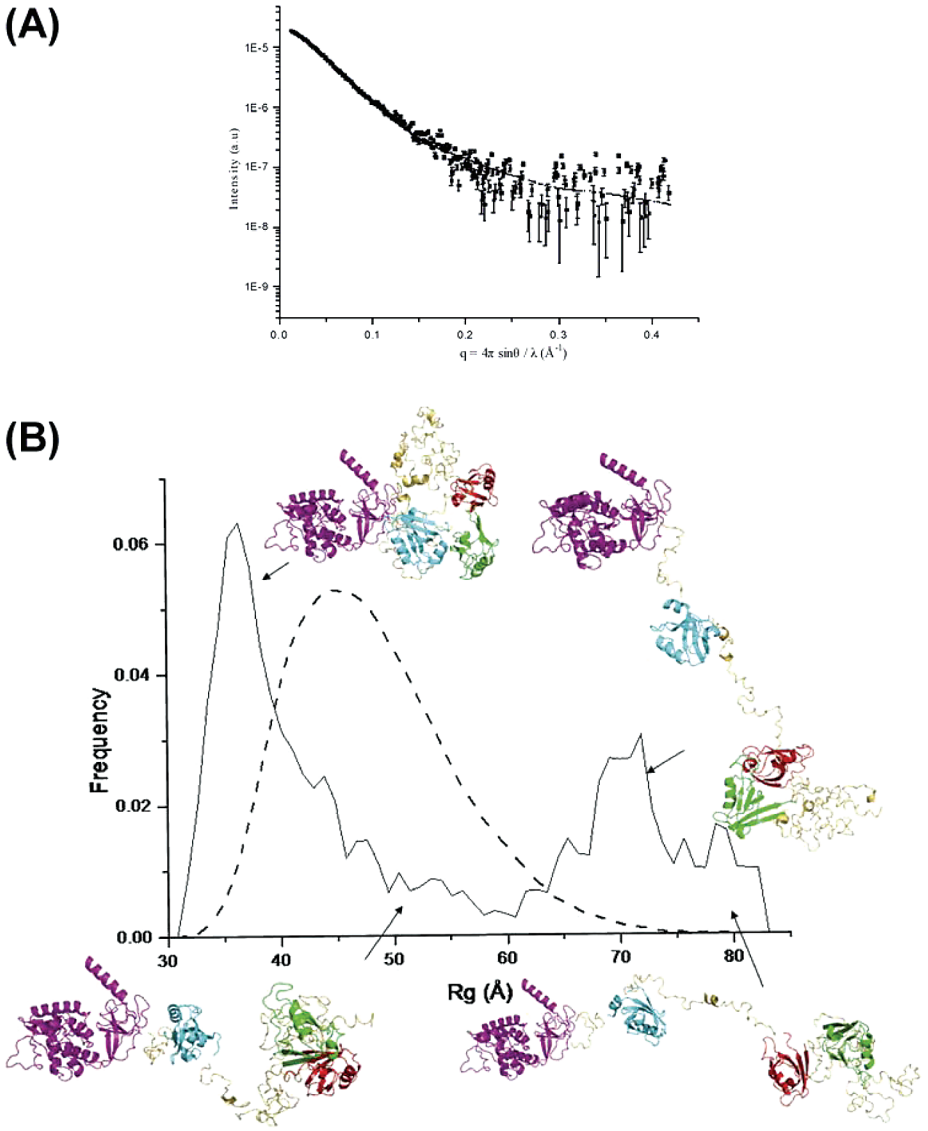

Figure 6. Analysis of SAXS data of Δ70 by the ensemble optimization method. (A) SAXS intensities plotted as a function of momentum transfer. Dots with error bars represent experimental data; the solid line represents the fit obtained from the ensemble of 14 conformers. (B) Distribution of the selected conformers (solid line) and the initial pool of random structures (dashed line) as a function of R_g. Four representative structures for the compact, semiextended, extended, and fully extended conformers within the EOM ensemble were assessed to realistically fit the Δ70 model. Color code: magenta for SH3-GK, cyan for PDZ3, brown for PDZ2, green for PDZ1, and yellow for the U1−U5 linker regions.

The SAXS data are consistent with the PDZ domain-containing region being mobile and support the model in which the PDZ region takes up different orientations and conformations with respect to the SH3-GK domain. Calculations using ensemble optimization of scattering data for Δ546 show that the SH3-GK domain is in a compact state. This is in agreement with the NMR data and with structures determined for SH3-GK domains from the homologous PSD-95. The many structures produced from the EOM calculations show negligible variations in the relative orientations of the SH3 domain with respect to the GK domain, with the elongated conformation due to the presence of the flexible 63-amino acid N-terminal region. Δ70 similarly exists as a mixture of compact and extended states. Interestingly, rather than a continuum of states, the calculations show that there is a discrete distribution of populations for Δ70, suggesting that there are constraints in the degree of freedom for the PDZ domains. The EOM structures also show that much of the elongation is due to the unravelling of the U3 and U4 linker regions. Our previous SAXS studies have also determined that the PDZ3 domain adopts a variety of locations with respect to the PDZ1 and PDZ2 domains, in agreement with our findings.[17]

The compact structures of Δ546 also show the *αβ* region of the U4 linker to be in the proximity of the SH3 domain. Superimposition of the compact EOM structures of Δ546 and Δ70 reveals similar spatial locations for the *αβ* region in both sets of structures. It is likely that the short *αβ* segment acts as a tether to restrict the dynamics of the U4 linker region and place the PDZ3 domain close to the SH3 domain. These results concur with previous reports that showed that PDZ3 forms functionally important interdomain interactions with the SH3-GK domain, although no structural information is available from those studies.[28] Our NMR and SAXS studies suggest that these intermolecular interactions are present but weak.

In the protein constructs used here, the U5 Hook linker region between the SH3-GK domain contains the I3 and I5

dx.doi.org/10.1021/bi201178v | *Biochemistry* 2012, 51, 899−908

splice insertions in addition to the helical Hook domain. The fact that the NMR line widths of the resonances from the whole SH3-GK region are similar, and different from the narrow line widths of the U5 Hook linker, implies that there are strong, stable interdomain interactions between the SH3-GK domains in SAP97 despite the linker region being longer than the PSD-95 SH3-GK domain. This strong interdomain SH3-GK interaction is also evident from the instability of the expressed, isolated GK domain and the significant shift differences between the isolated and intact GK domain. Preliminary data here also suggest little gross conformational change upon binding of CaM to the Hook region, again supporting the notion that the Hook domain is conformationally free to bind CaM without significantly affecting the overall structure of the SH3-GK domain.

Previous single-particle EM studies showed that full-length SAP97 adopts an elongated, rodlike conformation, with a minority (~35%) showing the more compact configuration that is similar to that adopted by PSD-95. Here we show that Δ70, which lacks the L27 domain, has a higher population of the compact form (52%). These results suggest that the L27 domain has a significant influence on the conformation of the SAP97 proteins. However, rather than existing predominantly in one compact conformation like other non-L27 MAGUK proteins such as PSD-95, SAP97 has more conformational heterogeneity, and this most likely is due to the presence of the additional long linker regions.

The results reported here, together with work done by other laboratories, suggest that the conformation of SAP97 is isoform-dependent. The L27 domain appears to have two effects on SAP97; it mediates SAP97 multimerization and also causes β-SAP97 to preferentially adopt an elongated conformation.[12] In the absence of L27, as is the case in the α-isoform, SAP97 is more compact and monomeric. The two isoforms have been reported to influence the recruitment, dynamics, and function of AMPA-type glutamate receptors (AMPARs) at the postsynaptic density as a result of the two isoforms being located in different parts of the postsynaptic region, with the β-form targeted mainly in the perisynaptic regions outside the postsynaptic density and the α-form being a core component of the postsynaptic density.[9] We propose here that this spatial distribution is accompanied by a conformational partitioning and that the role of SAP97 isoforms with respect to GluR1 function is influenced by the different conformations adopted by the MAGUK. The extended β-conformation may more readily bind target proteins because the binding sites are more accessible than in the compact form; on the other hand, being more compact, the α-form could require regulatory factors for binding to occur. It remains to be seen whether and how the different conformers of Δ70 affect its ability to simultaneously bind large receptors and ion channels

In summary, we have shown that the form of SAP97 that is equivalent to the α-isoform adopts compact and extended conformations, with the compact form being the more predominant one. We have also shown that the presence of flexile linker regions, with alternative splicing insertions, possibly contributes to the heterogeneous conformation of SAP97. The isoform-dependent distribution of SAP97 in the synapse may, therefore, reflect a separation of conformations, with the predominantly compact form located in the synapse and the extended form in the perisynapse. Future work is likely to focus on whether these conformational differences affect or influence function.

■ ASSOCIATED CONTENT

Supporting Information

Amino acid sequences of the various protein constructs, $^{1}H-^{15}N$ HSQC spectrum and secondary structure of SAPN, ab initio low-resolution 3D shape models of Δ546 and Δ70 reconstructed from the experimental scattering profile using GASBOR, and protein purification protocols. This material is available free of charge via the Internet at http://pubs.acs.org.

■ AUTHOR INFORMATION

Corresponding Author

*E-mail: Lu-Yun.Lian@Liverpool.ac.uk. Telephone: 0151 795 4458. Fax: 0151 795 4414.

Author Contributions

M.D.T. prepared the samples, performed the SAXS experiments, and analyzed the SAXS data. He also expressed labeled SAP97N and assisted with its ^{13}C, ^{15}N, and ^{1}H resonance assignment. M.P. collected the NMR spectra for SAPN and assigned its ^{13}C, ^{15}N, and ^{1}H resonances. S.P. prepared the labeled samples of Δ70, Δ461, and Δ546 and the samples for SEC–MALLS analyses. M.L. provided the constructs for all the proteins expressed in this study, and J.G.G. supervised the analyses of the SAXS data; they both assisted with writing the manuscript. L.-Y.L. directed the project, performed and analyzed the NMR experiments for Δ70, Δ461, and Δ546, and wrote the manuscript.

Funding

This work is supported by the University of Liverpool, which provided a studentship to M.D.T. and funds to support the NMR Centre for Structural Biology.

Notes

The authors declare they have no conflict of interest.

■ ACKNOWLEDGMENTS

SAXS beamtime at the SOLEIL beamline SWING is gratefully acknowledged. In particular, we thank Dr. Javier Pérez for his help and support during the acquisition of SAXS data at SWING. We also acknowledge Dr. Tom Jowitt and Ms. Marjorie Howard (Biomolecular Analysis Laboratory, Faculty of Life Sciences, The University of Manchester, Manchester, U.K.) for assistance with the MALLS experiments.

■ ABBREVIATIONS

AMPA, α-amino-3-hydroxy-5-methyl-4-isoxazolepropionic acid; EOM, ensemble optimization method; HSQC, heteronuclear single-quantum coherence; MAGUK, membrane-associated guanylate kinase; NMR, nuclear magnetic resonance; SAP97, synapse-associated protein 97; SAXS, small-angle X-ray scattering; TROSY, transverse relaxation optimized spectroscopy; SEC–MALLS, size exclusion chromatography–multi-angle laser light scattering.

■ REFERENCES

(1) Leonoudakis, D., Mailliard, W. S., Wingerd, K. L., Clegg, D. O., and Vandenberg, C. A. (2001) Inward rectifier potassium channel Kir2.2 is associated with synapse-associated protein SAP97. *J. Cell Sci. 114*, 987–998.

(2) Leonard, A. S., Davare, M. A., Horne, M. C., Garner, C. C., and Hell, J. W. (1998) SAP97 is associated with the α-amino-3-hydroxy-5-

methylisoxazole-4-propionic acid receptor GluR1 subunit. *J. Biol. Chem. 273*, 19518−19524.
(3) Bassand, P., Bernard, A., Rafiki, A., Gayet, D., and Khrestchatisky, M. (1999) Differential interaction of the tSXV motifs of the NR1 and NR2A NMDA receptor subunits with PSD-95 and SAP97. *Eur. J. Neurosci. 11*, 2031−2043.
(4) Lue, R. A., Marfatia, S. M., Branton, D., and Chishti, A. H. (1994) Cloning and characterization of hDlg: The human homolog of the *Drosophila* disks large tumour suppressor binds to protein 4.1. *Proc. Natl. Acad. Sci. U.S.A. 91*, 9818−9822.
(5) Nikandrova, Y. A., Jiao, Y. X., Baucum, A. J., Tavalin, S. J., and Colbran, R. J. (2010) Ca^{2+}/Calmodulin-dependent Protein Kinase II Binds to and Phosphorylates a Specific SAP97 Splice Variant to Disrupt Association with AKAP79/150 and Modulate α-Amino-3-hydroxy-5-methyl-4-isoxazolepropionic Acid-type Glutamate Receptor (AMPAR) Activity. *J. Biol. Chem. 285*, 923−934.
(6) Colledge, M., Dean, R. A., Scott, G. K., Langeberg, L. K., Huganir, R. L., and Scott, J. D. (2000) Targeting of PKA to glutamate receptors through a MAGUK-AKAP complex. *Neuron 27*, 107−119.
(7) McLaughlin, M., Hale, R., Ellston, D., Gaudet, S., Lue, R. A., and Viel, A. (2002) The distribution and function of alternatively spliced insertions in hD1g. *J. Biol. Chem. 277*, 6406−6412.
(8) Rumbaugh, G., Sia, G. M., Garner, C. C., and Huganir, R. L. (2003) Synapse-associated protein-97 isoform-specific regulation of surface AMPA receptors and synaptic function in cultured neurons. *J. Neurosci. 23*, 4567−4576.
(9) Waites, C. L., Specht, C. G., Hartel, K., Leal-Ortiz, S., Genoux, D., Li, D., Drisdel, R. C., Jeyifous, O., Cheyne, J. E., Green, W. N., Montgomery, J. M., and Garner, C. C. (2009) Synaptic SAP97 Isoforms Regulate AMPA Receptor Dynamics and Access to Presynaptic Glutamate. *J. Neurosci. 29*, 4332−4345.
(10) Godreau, D., Vranckx, R., Maguy, A., Goyenvalle, C., and Hatem, S. N. (2003) Different isoforms of synapse-associated protein, SAP97, are expressed in the heart and have distinct effects on the voltage-gated K^+ channel Kv1.5. *J. Biol. Chem. 278*, 47046−47052.
(11) Schluter, O. M., Xu, W. F., and Malenka, R. C. (2006) Alternative N-terminal domains of PSD-95 and SAP97 govern activity-dependent regulation of synaptic AMPA receptor function. *Neuron 51*, 99−111.
(12) Nakagawa, T., Futai, K., Lashuel, H. A., Lo, I., Okamoto, K., Walz, T., Hayashi, Y., and Sheng, M. (2004) Quaternary structure, protein dynamics, and synaptic function of SAP97 controlled by L27 domain interactions. *Neuron 44*, 453−467.
(13) Wu, H. J., Reissner, C., Kuhlendahl, S., Coblentz, B., Reuver, S., Kindler, S., Gundelfinger, E. D., and Garner, C. C. (2000) Intramolecular interactions regulate SAP97 binding to GKAP. *EMBO J. 19*, 5740−5751.
(14) Feng, W., Long, J. F., Fan, J. S., Suetake, T., and Zhang, M. J. (2004) The tetrameric L27 domain complex as an organization platform for supramolecular assemblies. *Nat. Struct. Mol. Biol. 11*, 475−480.
(15) Tavares, G. A., Panepucci, E. H., and Brunger, A. T. (2001) Structural characterization of the intramolecular interaction between the SH3 and guanylate kinase domains of PSD-95. *Mol. Cell 8*, 1313−1325.
(16) McGee, A. W., Dakoji, S. R., Olsen, O., Bredt, D. S., Lim, W. A., and Prehoda, K. E. (2001) Structure of the SH3-guanylate kinase module from PSD-95 suggests a mechanism for regulated assembly of MAGUK scaffolding proteins. *Mol. Cell 8*, 1291−1301.
(17) Goult, B. T., Rapley, J. D., Dart, C., Kitmitto, A., Grossmann, J. G., Leyland, M. L., and Lian, L. Y. (2007) Small-angle X-ray scattering and NMR studies of the conformation of the PDZ region of SAP97 and its interactions with Kir2.1. *Biochemistry 46*, 14117−14128.
(18) Konarev, P. V., Volkov, V. V., Sokolova, A. V., Koch, M. H. J., and Svergun, D. I. (2003) PRIMUS: A Windows PC-based system for small-angle scattering data analysis. *J. Appl. Crystallogr. 36*, 1277−1282.
(19) Semenyuk, A. V., and Svergun, D. I. (1991) GNOM: A program package for small-angle scattering data processing. *J. Appl. Crystallogr. 24*, 537−540.
(20) Svergun, D. I., Petoukhov, M. V., and Koch, M. H. J. (2001) Determination of domain structure of proteins from X-ray solution scattering. *Biophys. J. 80*, 2946−2953.
(21) Svergun, D., Barberato, C., and Koch, M. H. J. (1995) CRYSOL: A program to evaluate X-ray solution scattering of biological macromolecules from atomic coordinates. *J. Appl. Crystallogr. 28*, 768−773.
(22) Roy, A., Kucukural, A., and Zhang, Y. (2010) I-TASSER: A unified platform for automated protein structure and function prediction. *Nat. Protoc. 5*, 725−738.
(23) Petoukhov, M. V., and Svergun, D. I. (2005) Global rigid body modeling of macromolecular complexes against small-angle scattering data. *Biophys. J. 89*, 1237−1250.
(24) Bernado, P., Mylonas, E., Petoukhov, M. V., Blackledge, M., and Svergun, D. I. (2007) Structural characterization of flexible proteins using small-angle X-ray scattering. *J. Am. Chem. Soc. 129*, 5656−5664.
(25) Wishart, D. S., and Sykes, B. D. (1994) The C-13 chemical shift index: A simple method for the identification of protein secondary structure using C-13 chemical shift data. *J. Biomol. NMR 4*, 171−180.
(26) Chen, Y. H., Li, M. H., Zhang, Y., He, L. L., Yamada, Y., Fitzmaurice, A., Shen, Y., Zhang, H. L., Tong, L., and Yang, J. (2004) Structural basis of the $\alpha_1\beta$ subunit interaction of voltage-gated Ca^{2+} channels. *Nature 429*, 675−680.
(27) Van Petegem, F., Clark, K. A., Chatelain, F. C., and Minor, D. L. (2004) Structure of a complex between a voltage-gated calcium channel β-subunit and an α-subunit domain. *Nature 429*, 671−675.
(28) Newman, R. A., and Prehoda, K. E. (2009) Intramolecular Interactions Between the Src Homology 3 and Guanylate Kinase Domains of Discs Large Regulate Its Function in Asymmetric Cell Division. *J. Biol. Chem. 284*, 12924−12932.